Journal of Power Sources 223 (2013) 50–55

Contents lists available at SciVerse ScienceDirect

Journal of Power Sources

journal homepage: www.elsevier.com/locate/jpowsour

Facile synthesis of Sn/TiO_2 nanowire array composites as superior lithium-ion battery anodes

Zhen Wei, Han Mao, Tao Huang**, Aishui Yu*

Department of Chemistry, Shanghai Key Laboratory of Molecular Catalysis and Innovative Materials, Institute of New Energy, Fudan University, 2205 Songhu Road, Shanghai 200438, China

HIGHLIGHTS

- A novel material of TiO_2 nanowire array/Sn composite has been fabricated.
- The TNA–Li_2O framework ensures excellent cycling stability of the composites.
- Tin component brings high capacity and outstanding rate capability.

ARTICLE INFO

Article history:
Received 10 April 2012
Received in revised form
27 August 2012
Accepted 13 September 2012
Available online 18 September 2012

Keywords:
Titania nanowire array
Solvothermal crystal growth
Tin
Lithium-ion battery anode

ABSTRACT

A novel material of Sn/TiO_2 nanowire array (TNA) composite has been designed and fabricated to be used as anode material for lithium-ion batteries. Firstly, highly ordered, vertically oriented rutile TiO_2 nanowire array is synthesized directly on titanium substrate by solvothermal procedure without any template. Subsequently, tin metal is chemically deposited into the interspace of the film, forming a TNA/Sn composite. By calcinations in atmosphere, the skin-deep Sn is oxidized to SnO_2, and further turns to Li_2O in Li-ion insertion process. The field-emission scanning electron microscopy (FE-SEM) and transmission electron microscope (TEM) images indicate that the dimensions of TiO_2 nanowires and Sn particles are 10 ± 2 nm and 8 ± 1 nm wide, respectively. The energy-dispersive X-ray spectroscopy (EDX) result reveals that the weight ratio of tin to TiO_2 is 0.22. The first charge capacity reaches as high as 1610 mA h cm^{-3}, and the capacity retention is 62.3% after 300 cycles.

1. Introduction

Lithium-ion batteries (LIBs) have been considered the most promising energy storage technologies for mobile electronics, electric vehicles and renewable energy systems [1,2]. Among various anode materials, metal tin has attracted great attention for its unique properties. Its theoretical specific capacity (992 mA h g^{-1}, 7200 mA h cm^{-3}) is much larger than that of the already-commercialized graphite (372 mA h g^{-1}, 837 mA h cm^{-3}), and its discharge voltage plateau (0–400 mV) is a bit higher than lithium deposition voltage, needless of safety concern [3–5]. However, pure tin confronts a severe problem of volume expansion/contraction during the alloying and dealloying reaction with Li^+ [6], leading to the mechanical disintegration of the anode and loss of electrical connectivity between the active materials [7].

On the other hand, TiO_2 has small volume expansion ratio (3%) [8] upon intercalation/extraction of Li-ion, exhibiting good cyclic stability [9]. Well-ordered TiO_2 nanowire arrays offer a large internal surface area and excellent pathways for Li-ion to transfer between interfaces. However, the theoretical specific capacity of TiO_2 is very low (168 mA h g^{-1} for $Li_{0.5}TiO_2$), restricting its use in Li ion batteries. Recent report by Guanglei Cui [10] used a template-free strategy to prepare rutile TiO_2 nanowire arrays directly on a Ti foils substrate, and it shows a promising potential application in the Li-ion micro-batteries field. But the specific capacity is rather low, owing to the inherent characteristic of rutile TiO_2.

In this study, we design and fabricate a novel material of TiO_2 nanowire array (TNA)/Sn composite, which combines the advantages of high specific capacity of tin with the structural stability of TNAs. The TNA film is prepared via a non-polar solvent/hydrophilic substrate interfacial reaction under mild solvothermal conditions. Then tin metal is chemically deposited into the interspace of the film. The as-prepared TNA/Sn composite is already connected to titanium current collector, needless of binder and conductive agent

* Corresponding author. Tel./fax: +86 21 51630320.
** Corresponding author.
E-mail address: asyu@fudan.edu.cn (A. Yu).

0378-7753/$ – see front matter © 2012 Elsevier B.V. All rights reserved.
http://dx.doi.org/10.1016/j.jpowsour.2012.09.032

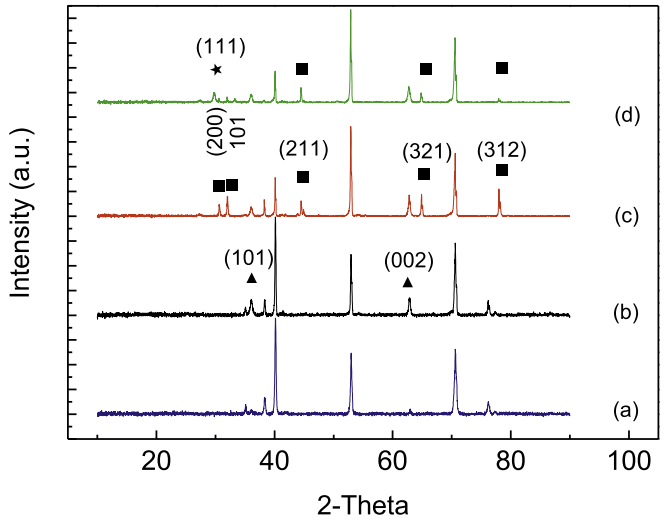

Fig. 1. XRD patterns of TiO_2 nanowire arrays and its composite with Sn: (a) titanium, (b) TNA, (c) sample A, and (d) sample B.

for Li-ion battery application. The stable volumetric capacity of TiO_2 improves as high as 312% by introducing tin component.

2. Experimental procedure

2.1. Material preparation

Pure titanium sheets with 14 mm in diameter and 0.3 mm in thickness were initially cleaned by ultrasonication in acetone, ethanol and deionized water for 30 min, respectively.

Before the solvothermal experiment, a compact TiO_2 nanoparticle layer was deposited onto the well-cleaned titanium substrate by being immersed in a 0.05 M $TiCl_4$ aqueous solution at 70 °C for 30 min, and then heated in air at 500 °C for 30 min [11]. We note that the TNA films without a compact layer tend to peel off from the substrate due to poor adhesion.

The titanium sheet was placed into a sealed Teflon autoclave (50 mL) with the surface treated by TiO_2 compact layer facing downward. Ten milliliters of toluene, 1 mL of tetrabutyl titanate and 1 mL of hydrochloric acid (37 wt %) were added into the autoclave as the solvothermal solution. The solvothermal process was

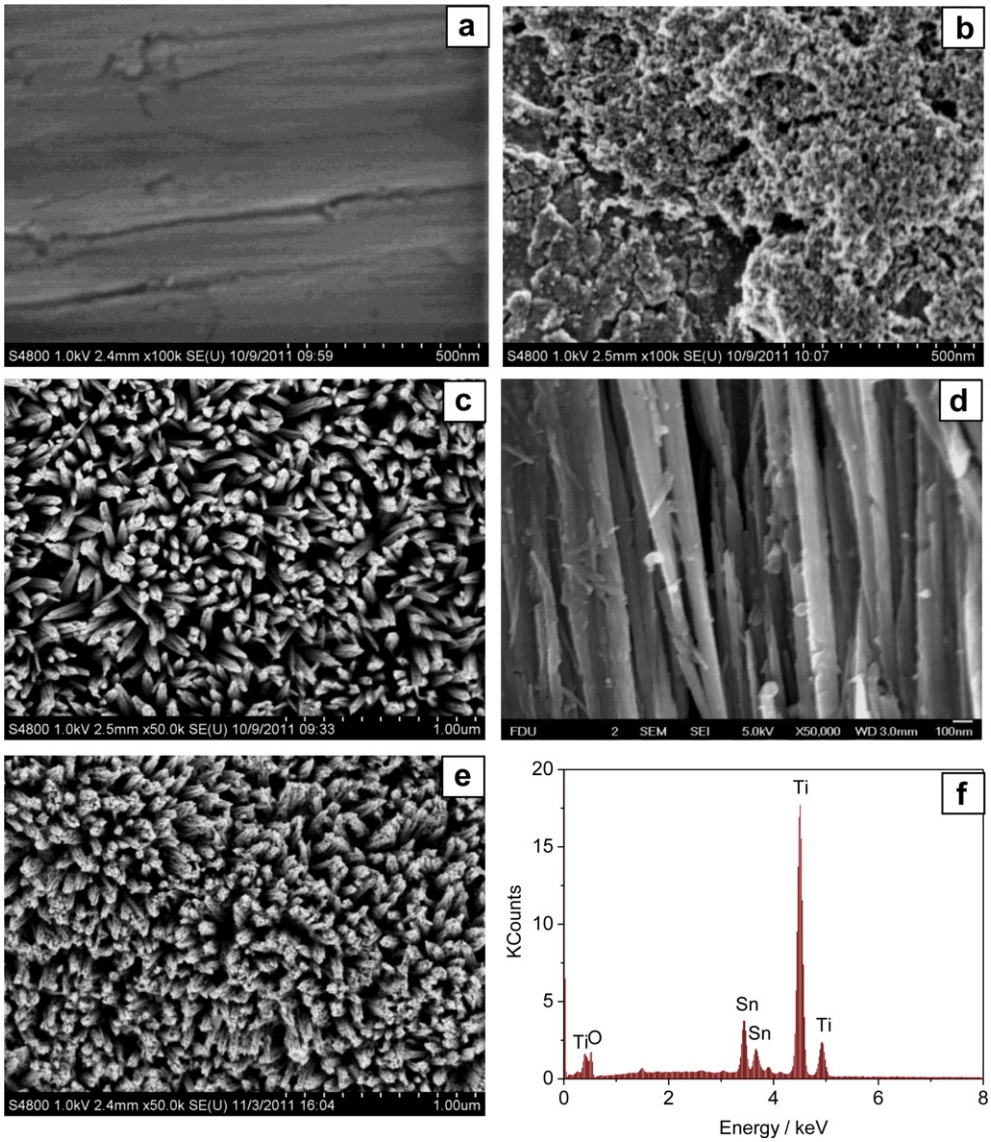

Fig. 2. FE-SEM images of the samples as prepared: (a) pure titanium substrate, (b) titanium substrate pretreated by 0.05 M $TiCl_4$ solution. (c, d) Top-view and cross-section of the TNA, (e, f) FE-SEM images of TNA/Sn composites and corresponding energy-dispersive X-ray spectroscopy.

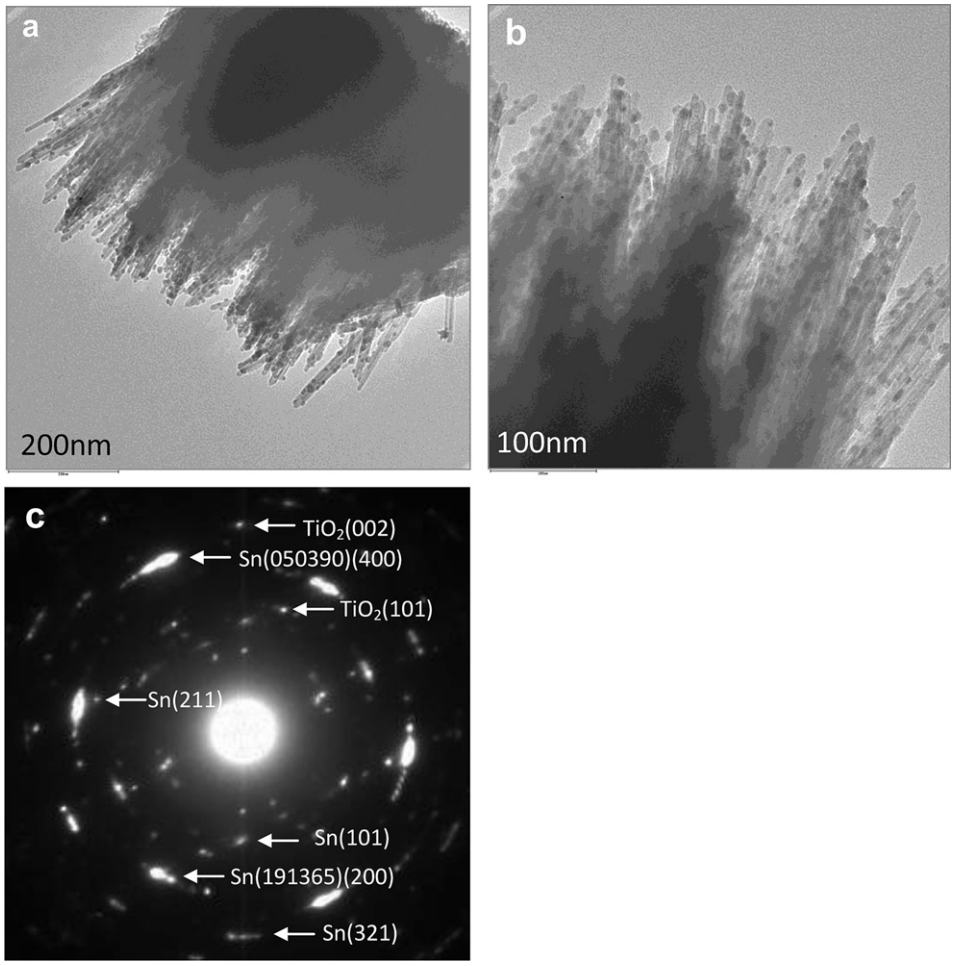

Fig. 3. TEM images of TNA/Sn composites: (a) low magnification and (b) high magnification.

conducted at 180 °C for 2 h in a furnace. After the solvothermal experiment, the resulting samples were rinsed with ethanol, and then dried in air.

Electroless plating of tin into the TNAs was achieved by a plating operation involving multiple sequences of sensitization, activation deposition of the copper and displacement of copper by tin. All the processes were carried out in a sonicating condition to ensure the reactions complete and uniform. The sensitizing solution consisted of 10 g L^{-1} $SnCl_2$ and 40 mL L^{-1} HCl. The TNAs were immersed in the sensitizing solution for 10 min, ensuring sufficient adsorption of Sn^{2+} on the surface of the nanowires. After being rinsed with deionized water, the TNAs were dipped into activation solution (20 g L^{-1} $AgNO_3$ + 500 mL L^{-1} ethanol) for 10 min. Ag^{+} was reduced to Ag, forming uniform Ag nanoparticles on the TNAs' surface. Meanwhile, Sn^{2+} was oxidized to Sn^{4+}. Electroless deposition of Cu was carried out in a commercial solution containing $CuSO_4$ and HCHO for 5 min. Finally, the Cu-coated TNAs were immersed in the electroless tin plating solution for 5 min to displace the Cu by Sn. Electroless tin plating solution was purchased from Weihai Runking Chemical Engineering Development Institute. It is a commercial solution containing tin salt, acid, complexing agent, reductive agent, surface active agent and so on. Complexing agent can coordinate Cu ion, change its potential versus tin. So with the help of complexing agent, reductive agent can reduce tin ion.

Two kinds of samples were fabricated for Li-ion battery application. Sample A: after deposition and washing, the TNA/Sn composite was directly used as battery anode. Sample B: the TNA/Sn composite was calcined at 180 °C for 24 h, and then used as battery anode.

After electrochemical discharge, sample B was taken out and washed with ethanol. Then it was calcined at 500 °C for 10 h in Ar/H_2 atmosphere, for XRD measurements.

2.2. Characterization and electrochemical measurements

The crystal structures of the samples were characterized by X-ray diffraction (XRD, Bruker D8 Advance) with Cu Ka radiation and selected area electron diffraction (SAED, TEM, JEM-2100F). The morphology was characterized using field-emission scanning electron microscopy (FE-SEM, Hitachi S-4800) and transmission electron microscope (TEM, JEM-2100F). The proportion of Sn to TiO_2 was determined by energy-dispersive X-ray spectroscopy (EDX, Hitachi S-4800).

Electrochemical tests were performed using a CR2016-type coin cell. The TNAs/Sn composites on Ti substrates were used directly as the working electrode. Cell assembly was performed in a glove box (Superstar 1220/750, Mikrouna) filled with pure argon. Lithium metal was used as counter electrode and the electrolyte was 1 M $LiPF_6$ dissolved in a mixed solvent of ethylene carbonate (EC)/diethyl carbonate (DEC) (1:1 by volume). A celgard 2300 membrane was used as the cell separator. Charge/discharge experiments were performed on a battery test system (LAND CT2001A, Wuhan Jinnuo Electronic Co. Ltd, China) between 0 V and 2.7 V at 150 mA cm^{-3}.

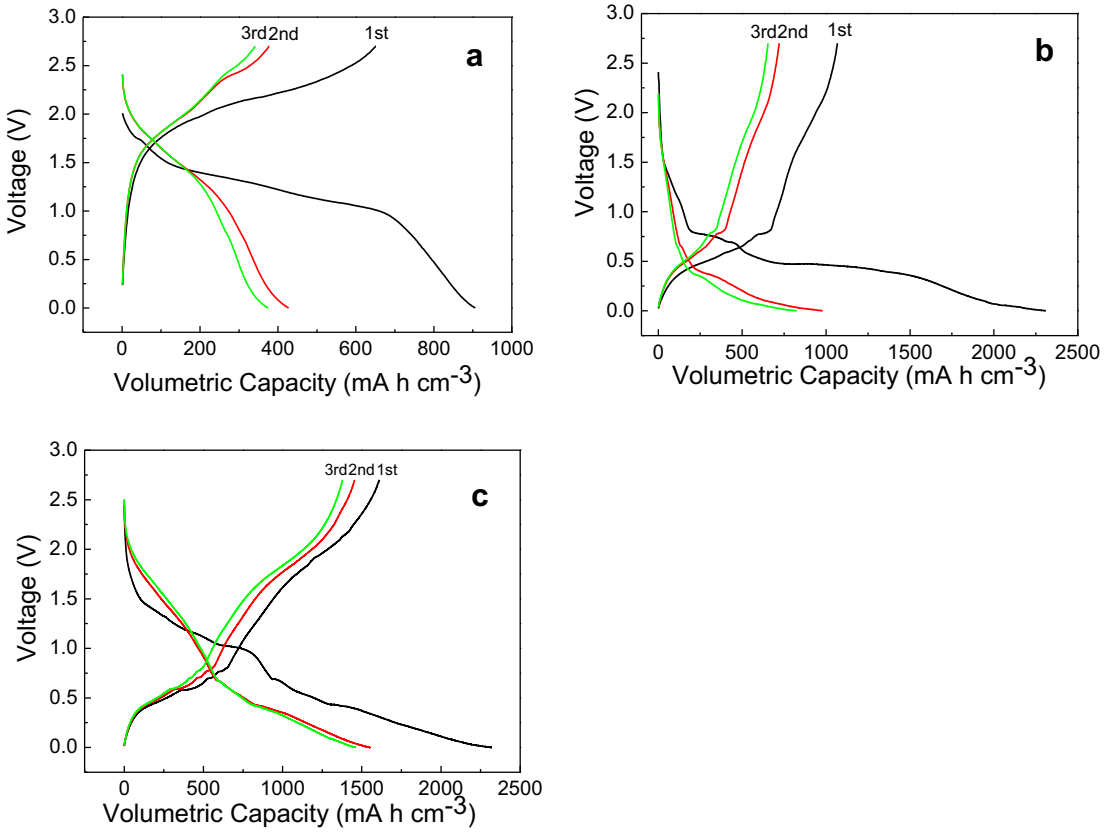

Fig. 4. The volumetric capacities of the initial three cycles: (a) TNA; (b) TNA/Sn composites without calcinations; and (c) TNA/Sn composites after being calcined at 180 °C for 24 h.

Weight of TiO_2 can be achieved by subtracting weight of Ti substrate from total weight of Ti/TiO_2, approximately 1.0 mg. The weight ratio of Sn to TiO_2 shown in EDX data is 0.22, so the weight of Sn is calculated as 0.22 mg, and weight of Sn/TiO_2 composite to be 1.22 mg. However, each weight is too small for balance to measure accurately. TNA grows on a titanium sheet and the titanium sheet is a circle shape with a diameter of 14 mm, so the area of TNA is $S = \pi \times (7\ \text{mm})^2 = 154.0\ \text{mm}^2$. The TNA film thickness was measured by a Veeco Dektak 150 Surface Profiler, $d = 1.6\ \mu\text{m}$ in average. The volume is calculated as $V = S \times d = 2.46 \times 10^{-4}\ \text{cm}^3$. In this paper, volumetric capacities (mA h cm^{-3}) are given because the applications of this novel nano-architectured electrode would be mostly thin film micro-batteries.

3. Results and discussion

Fig. 1(a) reveals the XRD patterns for Ti substrate and Fig. 1(b) for TNA on it. In Fig. 1(b), diffraction peaks (marked as "▲") at $2\theta = 36.1°$ and $2\theta = 62.7°$ are observed, which corresponds to the (101) and (002) crystal planes of rutile TiO_2 (JCPDS No. 21-1276). Fig. 1(c, d) shows the diffraction peaks of TNA/Sn composite, curve (c) for sample A and curve (d) for sample B. Apart from the peaks of rutile TiO_2, new diffraction peaks (marked as "■") emerge at $2\theta = 30.6°$, 32.0°, 44.9°, 64.6° and 79.5°, which ascribes to crystal planes (200), (101), (211), (321) and (312) of tin (JCPDS No. 04-0673), respectivley. No diffraction peaks for Cu are observed, illustrating that Cu is completely displaced by Sn. For TNA/Sn composites calcined at 180 °C for 24 h, as shown in Fig. 1(d), a new diffraction peak (marked as "★") at $2\theta = 29.9°$ is found, typical for the crystal face (111) reflection of the tin oxide (JCPDS No. 29-1484). However, the intensity of peak (111) is not strong, indicating that only the surface of Sn is oxidized to SnO_2.

Fig. 2 indicates the FE-SEM images of the samples prepared by solvothermal procedure. The surface of pure titanium substrate is glabrous and compact. The unit cell of hexagonal titanium ($a = b = 0.2951$ nm) does not match that of rutile TiO_2 ($a = b = 0.4594$ [12]), therefore, TNA can hardly grow directly on pure Ti metal. After pretreated by 0.05 M $TiCl_4$ aqueous solution, the titanium surface is coated by a very thin TiO_2 film, as shown in Fig. 2(b), and the film consisted of nanoparticles rather small and uniform. This film enables epitaxial nucleation and growth of rutile TiO_2, and also adhesion strength at the TiO_2 particles − TiO_2 nanowires are strong enough to avoid TNA peeling off from the Ti substrate.

After solvothermal reaction, as shown in Fig. 2(c) and (d), highly ordered, well-oriented TiO_2 nanowires are successfully fabricated, all growing perpendicular to the substrate. The essential structure of these samples is a single nanowire, and several nanowires bunch together to form a secondary structure, i.e. a bunch of nanowires. A single nanowire is 10 ± 2 nm wide, and the nanowire bunch is 60 ± 10 nm wide. In Fig. 2(e), after Sn deposition, the nanowire surface becomes rough and spotted, comparing with the glabrous image in Fig. 2(c), which illustrates that tin have deposited into the interspace between nanowires, and covers the surface of TiO_2 uniformly. The EDX spectrum in Fig. 2(f) proves the existence of Sn. The peaks of Sn are clearly seen, and quantitative analysis results show that the weight ratio of Sn:TiO_2 is 0.22. As for sample B, i.e. material after calcining in air atmosphere, there are no significant changes in FE-SEM images and EDX spectrum. No peaks of Cu are observed, indicating that Cu is displaced by Sn completely.

The nanowires/nanoparticles' structure is confirmed by TEM images and SAED pattern as shown in Fig. 3. It is clearly seen that dense dots distribute uniformly at the lateral surface of nanowires, proving that Sn particles have been successfully deposited into the interspace between the TiO_2 nanowires. High-magnification image

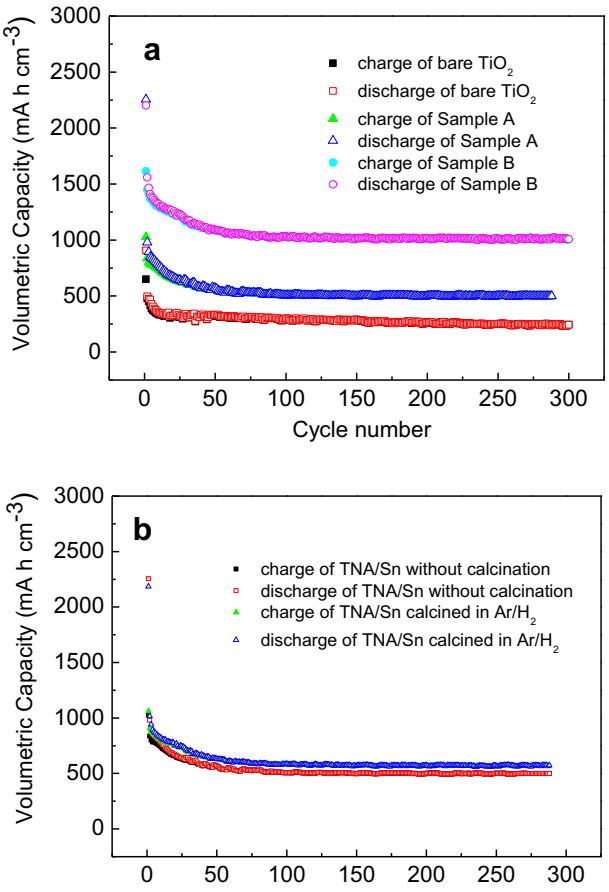

Fig. 5. (a) Cycle behavior of the electrodes made of bare TNA and TNA/Sn composites without/with calcinations. (b) Cycle behavior of TNA/Sn without calcination and calcined in Ar/H_2 atmosphere.

shows that the dimension of nanowire is 10 ± 3 nm wide, which corresponds to FE-SEM results. The Sn nanoparticles present itself structure of nanospheres with a diameter of 8 ± 1 nm. Fig. 3(c) confirms the crystalline structure observed in XRD pattern. Beside, more electron diffraction patterns appear, which are ascribed to crystal planes (400) of Sn (JCPDS No. 05-0390, gray tin) and (200) of Sn (JCPDS No. 191365). It is known that tin is very easily to convert to other crystalline structures, so several crystal patterns coexist in this material.

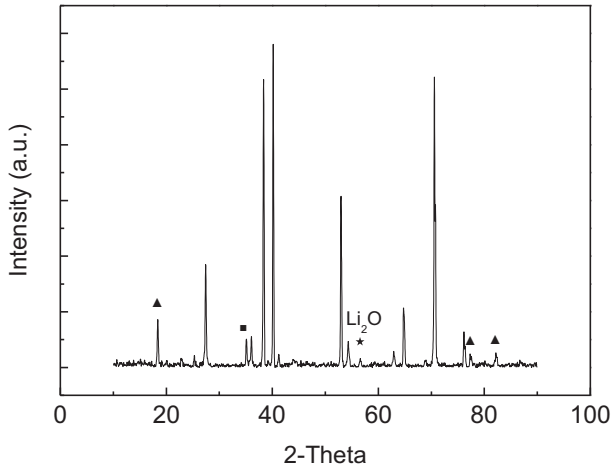

Fig. 6. XRD patterns of sample B after discharge and calcination.

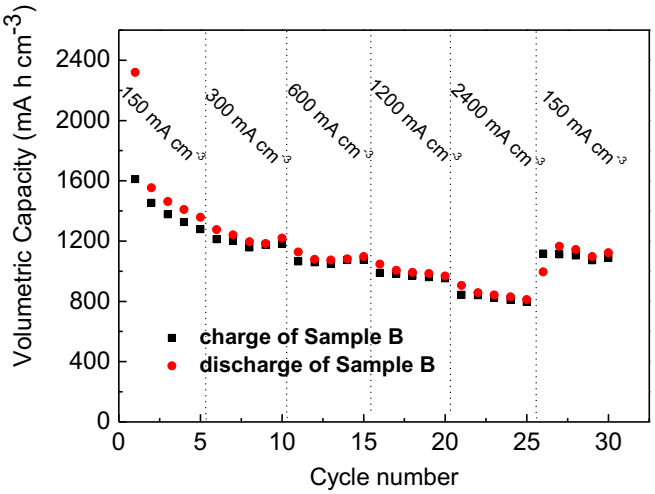

Fig. 7. Rate performance of TNA/Sn composites after calcinations at 180 °C for 24 h.

Galvanostatic charge–discharge measurement was performed to examine the electrochemical performance of the TNA film and TNA/Sn composite film as a lithium-ion battery electrode. Fig. 4 depicts the initial three cycles' volumetric capacities of these samples. The mass of the as-prepared samples is too small to weigh, so the lithium storage capacity is evaluated in volume. In average, the thickness of the TNA film measured by Surface Profiler is 1.6 μm.

The TiO_2 anode is always discharged to 1.0 V in previous works [13,14]. However, considering that tin-based materials are normally discharged to 0 V, in this study TiO_2 is also discharged to 0 V, as shown in Fig. 4(a). A sloping region in the range of 1.0–1.5 V during discharge and charge is visible. The slope behavior is consistent with that of nanosized rutile reported previously [9,15–17], which may be due to the Li surface storage of the rutile nanowires [15]. During the first cycle, a total discharge capacity of 906 mA h cm^{-3} is achieved with a reversible capacity of 651 mA h cm^{-3}, leading to a coulombic efficiency of 71.9%. For sample A shown in Fig. 4(b), apart from the discharge/charge plateaus of TiO_2, the potential plateau below 1.0 V versus Li/Li^+ is attributed to the intercalation/extraction of Li-ion in Sn. The TNA/Sn composite without calcinations shows an initial discharge capacity as high as 2308 mA h cm^{-3}, owing to large capacity of Sn. The initial reversible capacity is rather low, 1067 mA h cm^{-3}, corresponding to a coulombic efficiency of 46.2%. The reason for this low efficiency is that Sn exposes to the electrolyte directly, the huge volume expansion while Li-ion insertion can hardly recover, resulting in poor connection between Sn particles. As for sample B in Fig. 4(c), the TNA/Sn composite after calcinations exhibits an initial discharge capacity of 2320 mA h cm^{-3}, with a reversible capacity of 1610 mA h cm^{-3}, and the corresponding coulombic efficiency reaches as high as 69.4%. SnO_2 at the film surface is firstly reduced to Sn, accompany with the formation of Li_2O, shown in Eq. (1). Then Li-ion intercalation occurs in Sn to form Li_xSn alloy, shown in Eq. (2). It is generally accepted that the reaction in Eq. (1) is irreversible. Li_2O is electrochemically inert and distribute uniformly, constraining Sn in TiO_2 film and avoiding its expansion to electrolyte solution. Thus coulombic efficiency is improved significantly.

$$SnO_2 + 4Li^+ + 4e^- \rightarrow Sn + 2Li_2O \quad (1)$$

$$Sn + xLi^+ + xe^- \leftrightarrow Li_xSn (0 \le x \le 4.4) \quad (2)$$

By excluding 651 mA h cm^{-3} contributed by TiO_2, the first cycle charge capacity delivered by Sn is 959 mA h cm^{-3}.

Comparing the curves above 1.0 V in Fig. 4(b) and (c), the capacity contribution by TiO_2 in sample A is apparently smaller than that of sample B. This can be explained as follows. In TiO_2/Sn structure, the conductivity of Sn is much more superior than TiO_2, so current is much easier to get through Sn. Namely, the current is rarely distributed over TiO_2, so only a small amount of Li-ion intercalated into TiO_2. But in TiO_2/Sn/SnO_2 structure, the conductivity of SnO_2 is similar to TiO_2, so the current distribution over TiO_2 is largely improved and TiO_2 effectively exhibits its Li-ion insertion capacity.

Fig. 5(a) shows the cycling capacity values for the first 300 cycles. The rutile TNA electrode exhibits a good cycling stability and the charge capacity remains 244 mA h cm^{-3}, and capacity retention is 37.5% after 300 cycles. For TNA/Sn composite without and with calcinations, charge capacity after 300 cycles remains 48.5% and 62.3%, respectively. In particular, the reversible capacity of the calcined TNA/Sn composite anode after 300 cycles remains as high as 1006 mA h cm^{-3}, which is about 4 times of that of bare TNA anode (244 mA h cm^{-3}). By excluding the contribution of TiO_2, the 300th cycle reversible capacity of Sn remains 762 mA h cm^{-3}, which is 79.5% of the first cycle. The composite volume V is calculated as 2.46×10^{-4} cm^3, so the capacity contribution of tin is 0.1874 mA h . Regarding tin's mass as 0.22 mg and tin's density as 7.258 g cm^{-3}, its capacity is calculated to be 6200 mA h cm^{-3}, just a bit smaller than tin's theoretical capacity (7200 mA h cm^{-3}). The TNA/Sn composite after calcinations owns the best cycling stability. That is because the most capacity contribution is from Sn, and after calcinations, the unique TiO_2–Li_2O framework wraps Sn particles well, which can effectively lessen its volume expansion at Li-ion insertion process. As a result of excellent cycling stability of Sn, the TNA/Sn composite after calcinations owns even better capacity retention than bare TNA film, which enables itself a promising candidate for Li-ion battery electrode. Seen from Fig. 5(b), the cycle behavior of TNA/Sn composite is not improved by calcination in Ar/H_2 atmosphere, so the improvement on cycling stability is probably due to formation of SnO_2.

Fig. 6 shows the XRD patterns of sample B after discharge. Reaction resultants after electrochemical discharge are amorphous, and crystallized phase is achieved by calcination in Ar/H_2 atmosphere. The diffraction peak (marked as "★") at $2\theta = 56.4^\circ$ is typical for the crystal face (220) reflection of the lithium oxide (JCPDS No. 12-0254), which is a convincing evidence for the formation of Li_2O. Other reaction resultants are also observed. The diffraction peak (marked as "■") at $2\theta = 35.1^\circ$ ascribes to crystal planes (511) of $Li_{22}Sn_5$ (JCPDS No. 18-0753). Diffraction peaks (marked as "▲") at $2\theta = 18.4^\circ$, 77.5° and 82.4° correspond to the (003), (202) and (1011) crystal planes of $LiTiO_2$ (JCPDS No. 40-1053).

Fig. 7 reveals the performance of TNA/Sn composite with calcinations at rates varied from 150 mA cm^{-3} (corresponding to 0.1C) to 2400 mA cm^{-3} (corresponding to 1.6C). Reversible capacities of 1279, 1179, 1076, 952 and 796 mA h cm^{-3} are achieved at various rates. About 62.2% of the reversible capacity at 150 mA cm^{-3} remains while increasing current density to 2400 mA cm^{-3}. By reducing current density back to 150 mA cm^{-3}, the capacity recover to 1089 mA h cm^{-3}, which accounts for 85.1% of the initial capacity at 150 mA cm^{-3}. The excellent rate performance can be explained as follows: from XRD and FE-SEM data we can tell that TNA grows along (002) crystal plane, i.e. c-axis. During the process of Li-insertion into rutile TiO_2, the Li^+ diffusion coefficient is much higher along c-axis (10^{-6} cm^2 s^{-1}) than in the ab-planes (10^{-15} cm^2 s^{-1}) [18,19], the TNA structure in this study grows along c-axis, which significantly facilitates Li^+ diffusion. Besides, the Sn component is conductive. These two reasons enable good capability of rapid discharging and charging.

4. Conclusions

A novel material of TiO_2 nanowire array/Sn composite has been fabricated directly on titanium substrate through a facile method. This nanostructure provides good electrical contacts between the active materials and the current collector without using additives and conductive agents. The TNA–Li_2O framework ensures excellent cycling stability of the composite structure, and an appropriate amount of tin brings high volumetric capacity and outstanding rate capability. By introducing component of Sn, a reversible volumetric capacity increases significantly to 1610 mA h cm^{-3} for the initial cycle. The unique TiO_2–Li_2O framework accommodates Sn and lessen its mechanical strain during cycling. After 300 cycles, charge capacity remains 1006 mA h cm^{-3}, which is 4 times of that of bare TNA. The crystal growth direction of TNA and also electrical conductivity of Sn component facilitate rapid discharge/charge performance. Our study has therefore opened the great possibility for rutile TiO_2 nanowire arrays combined with other high capacity materials to apply in many fields of Li-ion batteries.

Acknowledgments

The authors acknowledge funding supports from the National Natural Science Foundation (No. 21173054) and Science & Technology Commission of Shanghai Municipality (No. 08DZ2270500), China.

References

[1] P.G. Bruce, B. Scrosti, J.M. Tarascon, Angew. Chem., Int. Ed. 47 (2008) 2930.
[2] D. Deng, M.G. Kim, J.Y. Lee, J. Cho, Energy Environ. Sci. 2 (2009) 818.
[3] S. Flandroisa, B. Simonb, Carbon 37 (1999) 165.
[4] P.G. Balakrishnan, R. Ramesh, T.P. Kumar, J. Power Sources 155 (2006) 401.
[5] L.G. Xue, Z. Wei, R.S. Li, J.L. Liu, T. Huang, A.S. Yu, J. Mater. Chem. 21 (2011) 3216.
[6] J. Wang, I.D. Raistrick, R.A. Huggins, J. Electrochem. Soc. 133 (1986) 457.
[7] N.C. Li, C.R. Martin, B. Scrosati, Electrochem. Solid-State Lett. 3 (2000) 316.
[8] M. Wagemaker, G.J. Kearley, A.A. Well, H. Mutka, F.M. Mulder, J. Am. Chem. Soc. 125 (2003) 840.
[9] D.H. Wang, D.W. Choi, Z.G. Yang, V.V. Viswanathan, Z.M. Nie, C.M. Wang, Y.J. Song, J.G. Zhang, J. Liu, Chem. Mater. 20 (2008) 3435.
[10] S.M. Dong, H.B. Wang, L. Gu, X.H. Zhou, Z.H. Liu, P.X. Han, Y. Wang, X. Chen, G.L. Cui, L.Q. Chen, Thin Solid Films 519 (2011) 5978.
[11] X. Feng, K. Shankar, O.K. Varghese, M. Paulose, T.J. Latempa, C.A. Grimes, Nano Lett. 8 (2008) 3781.
[12] C.J. Howard, T.M. Sabine, F. Dickson, Acta Crystallogr. Sect. B 47 (1991) 462.
[13] G.F. Ortiz, I. Hanzu, T. Djenizian, P. Lavela, J.L. Tirado, P. Knauth, Chem. Mater. 21 (2009) 63.
[14] G.F. Ortiza, I. Hanzua, P. Knautha, P. Lavela, J.L. Tirado, T. Djenizian, Electrochim. Acta 54 (2009) 4262.
[15] Y. Hu, L. Kienle, Y. Guo, J. Maier, Adv. Mater. 18 (2006) 1421.
[16] H. Qiao, Y. Wang, L. Xiao, L. Zhang, Electrochem. Commun. 10 (2008) 1280.
[17] B. Liu, E.S. Aydil, J. Am. Chem. Soc. 131 (2009) 3985.
[18] M.V. Koudriachova, N.M. Harrison, S.W. de Leeuw, Phys. Rev. Lett. 86 (2001) 1275.
[19] M.V. Koudriachova, N.M. Harrison, S.W. de Leeuw, Solid State Ionics 175 (2004) 829.